ACS APPLIED POLYMER MATERIALS

pubs.acs.org/acsapm

Article

Unclonable Features via Electrospraying of Bulk Polymers

Abidin Esidir, N. Burak Kiremitler, Mustafa Kalay, Alper Basturk, and M. Serdar Onses*

Cite This: *ACS Appl. Polym. Mater.* 2022, 4, 5952−5964

Read Online

ACCESS | Metrics & More | Article Recommendations | Supporting Information

ABSTRACT: The ability to encode unclonable information using low-cost materials and processes is of significant interest for anti-counterfeiting and information security applications. In this study, we present a versatile approach based on electrospraying of polymer solutions to generate randomly positioned complex features as a form of physically unclonable function (PUF). The key advantage of this approach is that readily available low-cost bulk polymeric materials can form small and complex features using a simple process. Polymers of varying composition and molecular weight, together with different solvents and electrospraying conditions, are systematically explored to construct the parameter space for PUFs of varying characteristics. Besides the randomness in the spatial positions and sizes of features, the key advantage of the presented approach is the ability to generate complex 3D shapes, which are very difficult, if not impossible to fabricate with the most advanced fabrication techniques. The inclusion of photoluminescent molecules establishes an additional security layer. The additive nature of operation enables multiplexing, *i.e.*, deposition of multiple materials on the same substrate. The fabricated PUFs have an average uniformity of 0.533 and uniqueness of 0.495, which are highly close to an ideal value of 0.5. The authentication is effectively performed using a feature detection algorithm without the need for markers and precisely defined rotation angles, greatly relaxing constraints associated with the imaging. Direct application of PUFs on the label of goods and authentication via a handheld microscope demonstrate the practical utility of the presented approach.

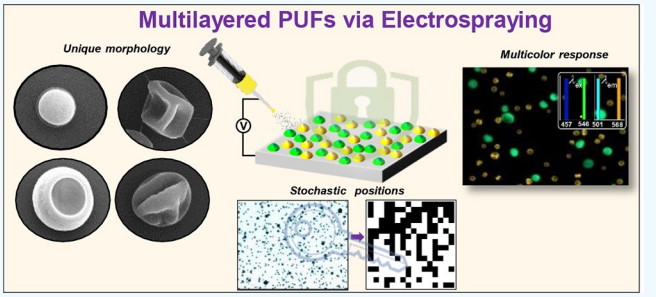

KEYWORDS: *physically unclonable function (PUF), electrospraying, polymers, fluorescence, encoding*

1. INTRODUCTION

Physically unclonable functions (PUFs) are receiving growing interest in a range of applications including anti-counterfeiting,[1] authentication,[2] supply chain tracking,[3] and internet of things.[4] PUFs rely on physical systems rather than digitized keys and are defined based on challenge-response pairs.[5] A physical system rather than a mathematical function is used to generate a response to a challenge. The physical system generates a unique and unclonable response to a challenge. The uniqueness and unclonability emerge from the stochastic physical process used to construct PUFs.[6] Randomness in the spatial position of features is a commonly used approach to construct PUFs. A broad range of materials and authentication systems has been studied for PUF applications. Examples include, carbon nanotubes,[7] microlenses,[8] nanogels,[9,10] nanoflakes,[11] nanoislands,[12] nanowires,[13] silk,[14,15] nanodiamonds,[16] lanthanide-doped zeolites,[17] quantum dots,[18,19] and perovskite nanocrystals.[20−23] A common characteristic of these studies is that they use different forms of nanoscale and microscale particles. Despite the unique properties and appealing characteristics of these materials, there are practical issues that relate to the cost and scalable manufacturing of such PUFs for industrial applications. These issues strongly motivate fabrication of PUFs using inexpensive and bulk materials. Polymers are particularly attractive materials for PUF applications not only for their low cost but also for their recyclability as effectively demonstrated in a recent study by Sørensen and co-workers.[24] It is highly desirable to generate PUFs constructed from microscopic and nanoscopic features with complex morphology, which are fabricated in one step at room temperature from bulk and low-cost materials.

Electrohydrodynamic instabilities are common in nature and also utilized in engineering applications.[25−27] Electrospinning, for example, is an effective means of generating nanoscale fibers.[28,29] The whipping instability is responsible for the random orientation of nanoscale fibers. Previous studies have shown that such nanoscale fibers can be used for encoding;[30−33] however, the continuous form of fibers poses challenges in their adaptation for generating randomly positioned discontinuous features. Electrospraying is a particularly interesting electrohydrodynamic process to generate randomly positioned isolated features. The chaotic nature of this instability offers a highly suitable platform for generating random features. When a steady

Received: May 11, 2022
Accepted: June 20, 2022
Published: June 30, 2022

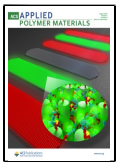

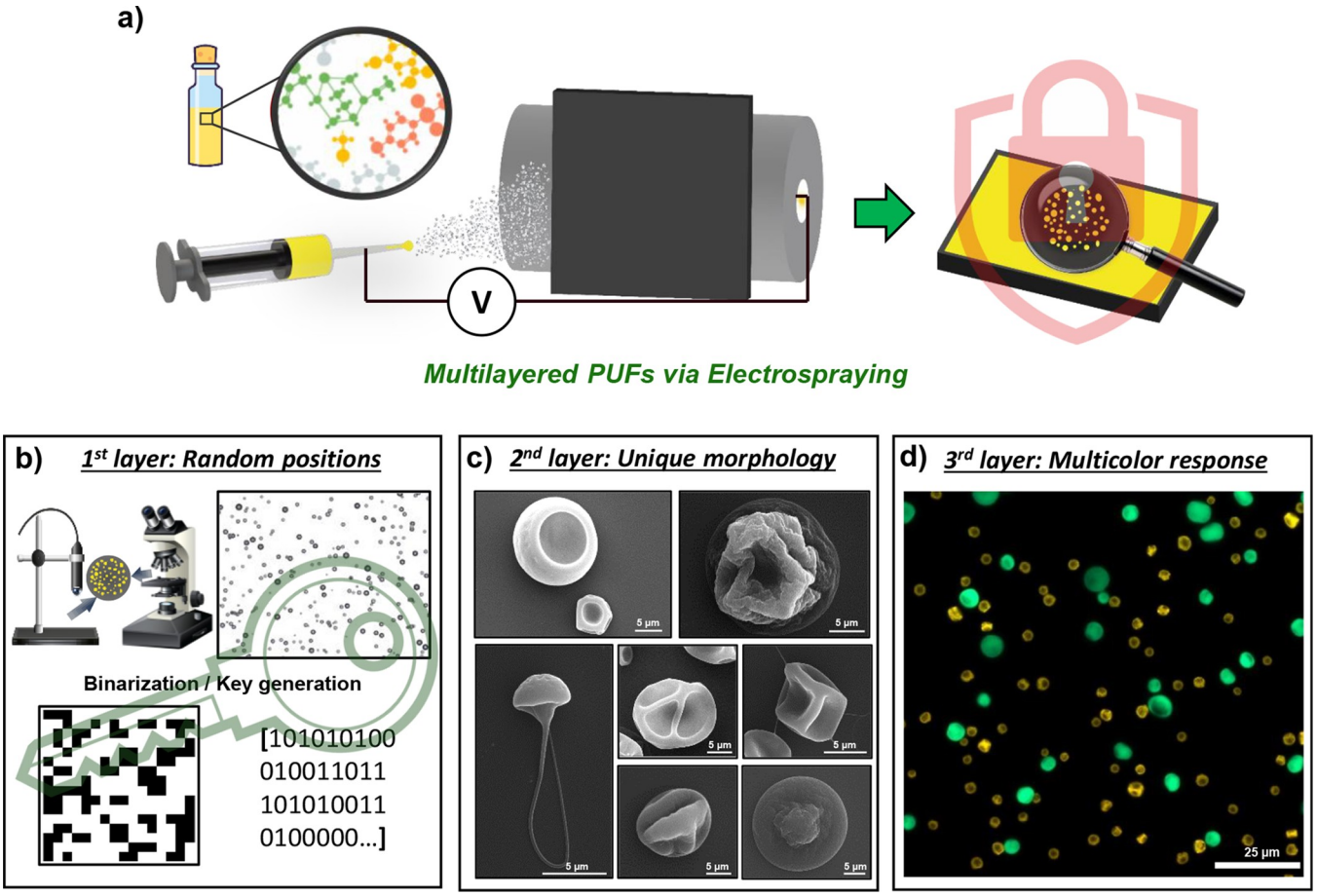

Figure 1. Generation of multilayered PUFs using electrospraying. (a) Schematic description of the process. (b) The first security layer is based on randomly positioned features. (c) The second security layer is formed by the complex and unique features, which can be obtained as a function of the polymer chemistry, solvent, polymer concentration, and electrohydrodynamic conditions. (d) The photoluminescent molecules can be incorporated within polymers establishing the third security layer, which is authenticated via a fluorescence microscopy image.

cone-jet[34] is achieved by the appropriate polymer solution and operating parameters, solid features with sizes that range from the micrometer to nanometer scale can be obtained. Thanks to the acting Coulomb repulsion to the droplets during electrospraying, these droplets can self-separate without being agglomerated, and the positions on the surfaces are random due to the chaotic trajectories they follow.[25,35] Inspired by the inherently stochastic nature, we propose electrospraying as a universally applicable fabrication method for the generation of unclonable features for PUF applications. In one example, Young and co-workers[36] used electrospraying as a form of deposition of quantum dots over a drop-cast layer of gold nanoparticles coated with titanium dioxide films to study the formation of hot-spots for PUF applications. To the best of our knowledge, electrospraying of bulk polymers to fabricate PUFs has not been reported.

In the following, we present low-cost, scalable, and room temperature fabrication of PUFs composed of micrometer- and nanometer-scale features via electrospraying of bulk polymeric materials. The direct use of low-cost materials with industrial scale availability is a key aspect of the presented study. The cost of polystyrene, for example, is about $1000 per metric ton. We systematically study polymers, solvents, and electrohydrodynamic conditions to reveal their effects on the size, structure, and surface coverage of features. The detailed study of parameter space with different polymers reveals the processing condition structure relationship for PUF studies. In addition to the randomness in the spatial position of features, their complex 3D morphologies establish an unclonable security layer. Such morphologies are almost impossible to imitate using conventional fabrication techniques. We demonstrate that photoluminescent molecules can be readily included in the electrospraying solution to confine them within unclonable features. The additive operation enables easy multiplexing without damage to the formerly deposited materials. In addition to the analysis of PUF characteristics including uniformity, uniqueness, and randomness, we show that a range of feature extraction algorithms can be used for authentication. Finally, an application on the label of a smartphone is demonstrated through authentication with a feature matching algorithm.

2. RESULTS AND DISCUSSION

2.1. Fabrication of Unclonable Features of Varying Sizes via Electrospraying. This work proposes facile fabrication of microscopic and nanoscopic unclonable features through electrospraying of polymer solutions. Figure 1 presents schematic illustrations and key results. The first step consists of the preparation of a polymer solution using the polymers and solvents presented in Tables 1 and 2. The polymer solution is then directly electrosprayed on the substrate (Figure 1a). Despite the involvement of electric fields, the process can be executed on insulators by using a conducive support. During the

https://doi.org/10.1021/acsapm.2c00803
ACS Appl. Polym. Mater. 2022, 4, 5952−5964

Table 1. Polymers, Their Acronyms, and Molecular Weights

acronym	polymer	molecular weight (kg/mol)
PEO35K	poly(ethylene oxide)	35
PVP360K	polyvinlypyrollidone	360
PVP1300K	polyvinlypyrollidone	1300
PMMA120K	poly(methyl methacrylate)	120
PMMA350K	poly(methyl methacrylate)	350
PS35K	polystyrene	35
PS280K	polystyrene	280
P2VP40K	poly(2-vinlypyridine)	40

Table 2. Solvents, Their Acronyms, and Key Properties[a]

acronym	solvent	dielectric constant (ε)	boiling point (T_{bp}) (C°)	ε/T_{bp} (1/°C)
CB	chlorobenzene	5.62	132	0.0425
DMF	*N*,*N*-dimethylformamide	36.7	152	0.2410
CB/DMF	CB/DMF (9/1 v/v)	~8.73	~132	0.0640
CHF	chloroform	4.82	61	0.0790
DCM	dichloromethane	8.93	40	0.0223
DW	water	80.1	100	0.8010
DW/ETH	DW/ethanol (1/1 v/v)	~52.3	~89	0.5880

[a]Dielectric constants of mixtures calculated by the equation of $\varepsilon_m = \varphi_1 \cdot \varepsilon_1 + \varphi_2 \cdot \varepsilon_2$.[44]

process of electrospraying, the polymer solution is fed through the needle. Applying an electric field between the needle and collector above a threshold value accumulates the electric charge carriers to the apex of the conical-shaped solution.[37] Subsequently, electrical forces overcome the surface tension of the solution, resulting in the emergence of an electrically charged thin liquid jet. Due to Rayleigh instability, this jet breaks up into droplets.[25,34,38] This type of instability is critical in the stochasticity of the process. These droplets simultaneously undergo evaporation of the solvent that leads to the deposition of polymeric features at random positions. This randomness essentially emerges from the electrohydrodynamic instability and chaotic trajectories followed by the droplets. After the jet formation, the Coulombic repulsion force acting on the charged droplets provides self-dispersion, as well as the intertwined complex effect of the drag and gravitational forces, causing these droplets/particles to randomly immobilize on the surface.[39,40] The randomly positioned droplets form a unique pattern on the surface. The pattern is unclonable, and even the operator cannot repeat these patterns. The randomly positioned polymeric features establish the first layer of PUF. This first layer (Figure 1b) can be visualized by simple optical imaging, and the resulting images can be used to construct binary keys. The length scale of the unclonable features is suitable for authentication via handheld microscopes overcoming the need for a complex and costly infrastructure. To further enhance the applicability, high-end smartphones with proper lenses or modifications can also be

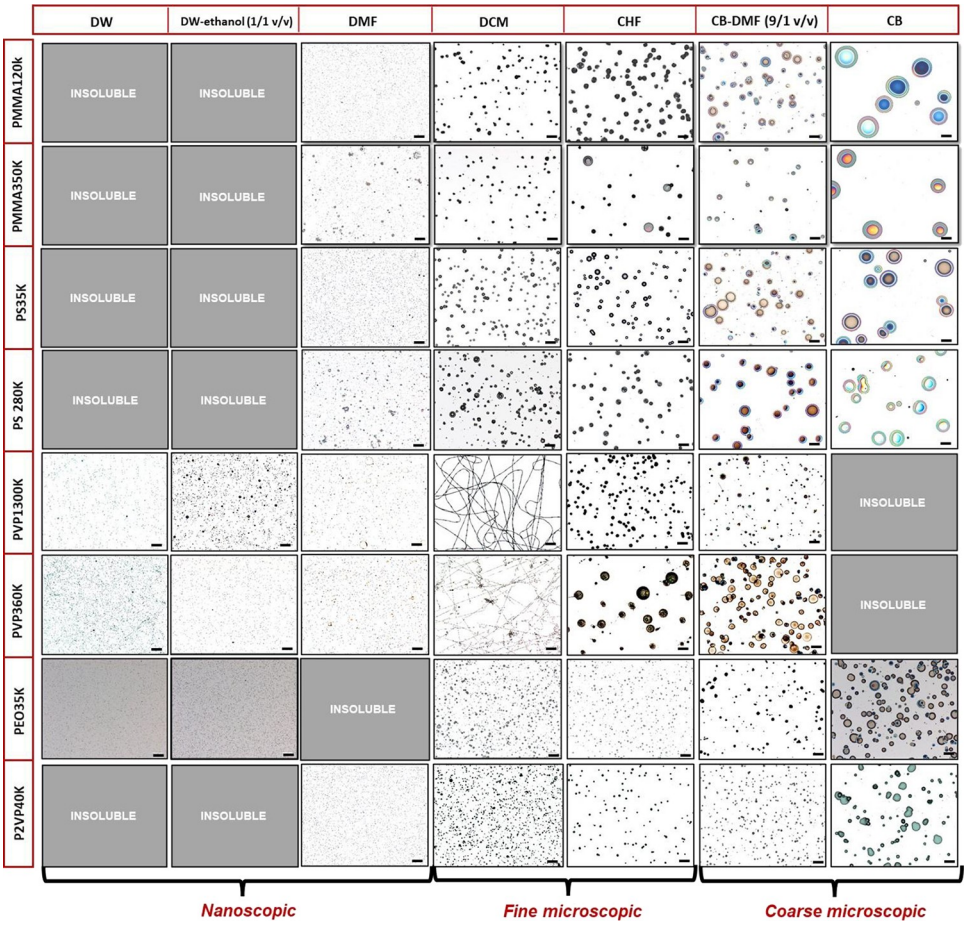

Figure 2. Size and morphology of features as a function of the polymer and solvent (scale bars: 50 μm). See Tables 1 and 2 for the full names of the polymers and solvents.

https://doi.org/10.1021/acsapm.2c00803
ACS Appl. Polym. Mater. 2022, 4, 5952−5964

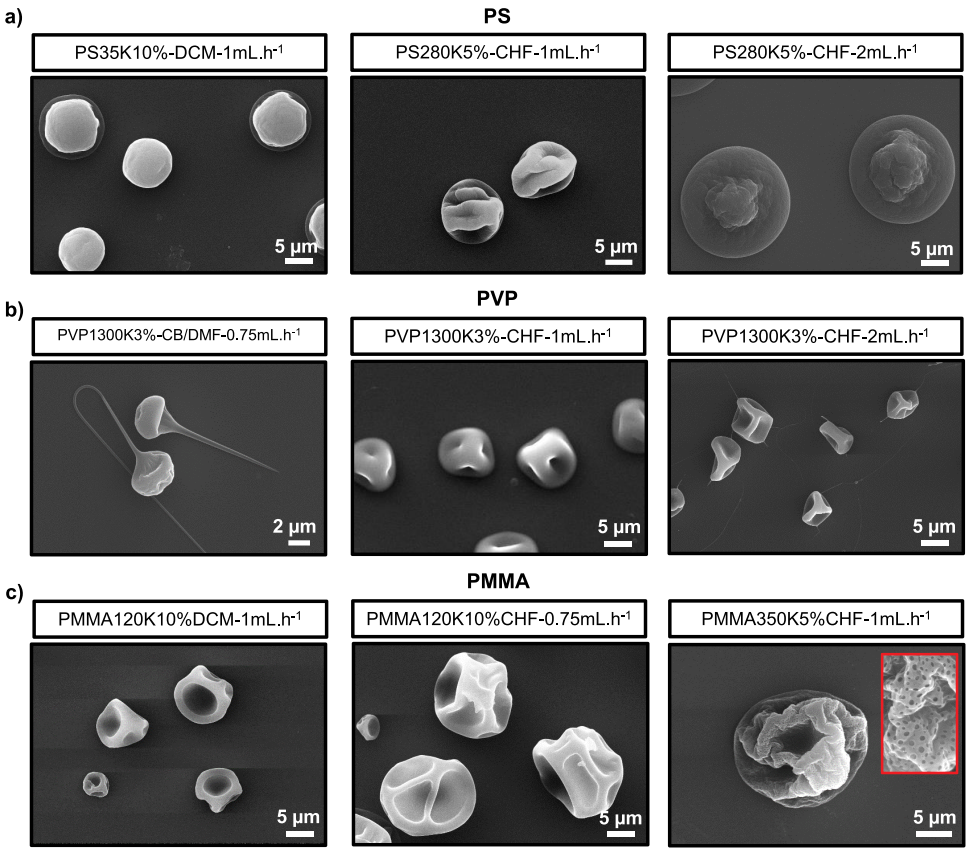

Figure 3. Generation of random structures with different morphologies. SEM images of structures electrosprayed from solutions of (a) PS, (b) PVP, and (c) PMMA. Abbreviations for electrospray parameters are given above each image. For example, the expression PMMA350K5%CHF-1mL·h^{-1} refers to the electrospraying of a chloroform solution of PMMA with a molecular weight of 350 kg/mol at a 5% concentration and a feed rate of 1 mL/h.

used.[41,42] Such keys can be formed at the point of manufacturing and stored in a digital database. To probe the authenticity of a product, the key obtained at the inspection could be simply compared with the key in the digital database. Advanced forms of authentication via image matching algorithms are possible and described in the following sections. In addition to the randomness in the position of polymeric features, their complex morphology can be used for encoding. As an example, SEM images of polymeric features with different types of morphology are given in Figure 1c. The complex, curved, and 3D nature of these microscopic features make them very difficult, if not impossible to duplicate using conventional fabrication techniques. The solution processing-based fabrication allows for the incorporation of functional materials into polymeric features and enables the formation of additional security layers. We demonstrate this concept through the addition of photoluminescent molecules. The resulting features can be resolved using a fluorescence microscope (Figure 1d). Note that the complex morphology of the features is even attainable from the fluorescence microscopy images. The additive operation of electrospraying is highly advantageous in terms of multiplexing, *i.e.*, the deposition of multiple materials with different properties. The proposed PUF system is layered, and each layer is defined by a different challenge-response pair. The challenge of the first layer is optical microscopy imaging, which results in a response that consists of randomly positioned polymeric features. In the second layer, the system can be challenged by using an electron microscopy. The response is formed by the complex morphology of the polymeric features. In the third layer, fluorescence microscopy imaging is used as a challenge. The unique fluorescence from the randomly positioned photoluminescent molecules constitutes the response of this third layer. This first and third layer can be read relatively fast, on the order of seconds. The second layer can be utilized in advanced security systems, and read can take as long as tens of minutes.[43]

The capability of fabricating randomly positioned features with a broad range of sizes at different length scales is significant for PUF applications.[12] Microscopic (>1 μm) features can be authenticated using portable cameras and even smartphones, making the technique accessible.[2,24] Nanoscopic features are suitable for high-end applications, where the authentication can be performed via advanced microscopy techniques such as SEM[43] and atomic force microscopy (AFM)[12] as recently demonstrated. Considering the need for infrastructure and read time, such nanoscopic features can be utilized as additional security layers for valuable products and documents. In this context, electrospraying offers critical capabilities. To explore these capabilities, we studied a range of polymers and solvents for generating randomly positioned features using electrospraying. Polymers (PS, PMMA, P2VP, PVP, and PEO) with five different backbone chemistries were used for electrospraying. Different molecular weights were studied for PS, PMMA, and PVP. The solution and operation parameters were investigated in detail to generate unclonable features of varying sizes and morphologies. The upper and lower limits of the concentration of the polymer were chosen in a range to prevent the formation of nanofibers and deposition of sessile droplets. Suitable concentrations of the polymer solutions were determined to be 5% for PS280K, 10% for PS35K, 10% for both PMMA120K and PMMA350K, 0.5−3% w/w for PEO35K,

https://doi.org/10.1021/acsapm.2c00803
ACS Appl. Polym. Mater. 2022, 4, 5952−5964

3% w/w for PVP, and 30% w/w for P2VP40K. Well-separated features were successfully obtained from electrosprayed solutions prepared within this concentration range (Figure S1).

Figure 2 summarizes the results obtained by electrospraying of the polymers using different solvents. The unclonable features were classified into three groups based on their sizes. The coarse microscopic refers to the features with critical dimensions larger than 15 μm. The nanoscopic class was defined for features with critical dimensions smaller than 1 μm. The fine-microscopic class covers the length scales in between the two other classes. In Figure 2, each column refers to a different solvent and each row refers to a polymer of a particular molecular weight. The solvent is a critical parameter affecting the size and morphology of features. This observation is well supported with the importance of the solvent in various electrohydrodynamic processes.[25,45,46] The dielectric constant and boiling point (*i.e.*, volatility) are particularly critical intrinsic properties of the solvent. As a general trend, the size of the features decreased from microscopic to nanoscopic dimensions, with an increase in the ratio of the solvent dielectric constant to the solvent boiling point (ε/T_{bp}; Table 2). CB, for example, has a significantly low dielectric constant (ε = 5.62) and high boiling point (T_{bp} ~132 °C) with a ε/T_{bp} of 0.0425 °C^{-1}, and the resulting features are large (coarse microscopic). The addition of a small amount of DMF results in a solvent mixture (CB-DMF 9/1 v/v) with a slight increase in ε/T_{bp} to a value of 0.064 °C^{-1}, which leads to a decrease in the size of the features. Solvents (CHF and DCM) with medium dielectric constants and low boiling points yielded spherical/hemispherical features with sizes that range from 1 to 15 μm (fine microscopic). Generally, the size of the features obtained from the same polymer by using CHF is larger than DCM. Meanwhile, solvents (DMF, DW-ethanol (1/1 v/v), and DW) with high dielectric constants and boiling point resulted in features with sizes as small as 50 nm (nanoscopic). Solutions of PS35K-CHF, PVP1300K-DW-Ethanol, and PEO200K-DW resulted in featureless spherical particles with average widths of 14.0, 1.0, and 170 nm, respectively. SEM images of the features and their size distribution are provided for representative cases in Figure S2. The flow rate is another important parameter to tune the size of features in electrohydrodynamic processes.[25,34,47] The size of features increased with the increasing flow rate for different concentrations of polymers and also polymers functionalized with fluorescent molecules (Figures S3 and S4).

The wetting properties of these polymers span a broad range from hydrophilic to hydrophobic. Some of these polymers are low cost and produced at industrial scales, whereas others include functional chemical groups offering routes for post-modification. These characteristics are important to meet the diverse requirements of PUF applications. The PS and PMMA are hydrophobic and mostly inert polymers. PVP and PEO are hydrophilic, biocompatible, and biodegradable polymers.[48,49] P2VP can form strong electrostatic bonds with many different nanomaterials, thanks to the pyridine group.[50−52] Collectively, these results position the electrospraying as a versatile approach for the fabrication of high performance PUFs.

2.2. Complex Features. The randomly positioned features generated by electrospraying can exhibit complex morphologies depending on the processing conditions. This capability provides a key opportunity for constructing a second security layer based on the sub-microscopic structure of the features. In this scheme, each feature itself possesses unclonable information defined by the morphology. Note that complex morphologies such as wrinkling are widely utilized as a form of encoding, including the natural fingerprints of humans.[53,54] Figure 3 presents a range of different morphologies obtained by PS, PVP, and PMMA by simply changing the molecular weight of the polymer, solvent composition, concentration of the polymer, and flow rate. These results imply that a plethora of morphologies can be achieved with the proposed approach. In the case of PS, the morphology varies from plain spherical to lip-like and outspread button-like features (Figure 3a). Similar morphology transitions are observed for polymers with different chemistries. When PVP dissolved in a mixture of solvents is used in electrospraying, nail-like features consisting of a bead with a fiber tail were obtained (Figure 3b). Using chloroform or dichloromethane as the solvent resulted in buckled, wrinkled, or cup-like features. Hollow features with polygonal structures were observed for PMMA (Figure 3c). In this case, using a low polymer concentration with a solvent with high volatility resulted in nanoscale pores on the features.

The morphology of the electrosprayed features is highly dependent on the properties of the solvent and polymer. As the solvent evaporates from the initial droplet, the degree of developed mechanical mismatch between the inner and external layers of the droplet is an essential factor that defines the intrinsic morphology.[25] The reason for the formation of plain spherical particles for PS10% (Figure 3a and Figure S2c) is that the external shell has a sufficient elastic modulus against the compressive stress and uniaxial precipitation of macromolecular chains formed between the inside and outside of the precursor droplet during the evaporation of the solvent. The morphology transitions observed at low polymer concentrations can be mainly attributed to insufficient chain entanglement. Accordingly, due to the low concentration, slightly or moderately buckled structures formed (Figure 3a). The formation of the characteristic microcup morphology depends on the delicate balance between the properties of the polymer and solvent. This balance depends on how well the solvent dissolves the polymer and the conductivity and surface tension of the resulting solution. In the case of PMMA, for example, DCM results in the formation of cup-like features (Figure 3c), whereas such features are absent in CHF using similar conditions. Rather highly wrinkled structures have formed due to the excessive deflection of initial droplets (Figure 3c), and the average size of the structures has increased using CHF. This contrast between DCM and CHF can be explained in the light of two factors. First, DCM is a better solvent for PMMA than CHF, as can be identified by the Hansen space parameter (R_a).[55,56] For the case of PMMA120K-DCM, the calculated R_a value is lower (3.58 MPa$^{0.5}$) than PMMA120K-CHF and PMMA350K-CHF (7.78 MPA$^{0.5}$), indicating that polymer chains in the PMMA-DCM system disperse better, thus yielding enhanced viscosity. Second, the dielectric constant, conductivity, and surface tension are higher for DCM (γ_s = 27.8 and 26.7 mN·m^{-1} for DCM and CHF, respectively), resulting in smaller particles. By the combination of these properties, the specific cup-like precipitation has occurred. Note that the employed conditions were in the only-bead regime of the electrospraying, and the mechanical properties of the initial droplet did not allow excess Coulombic fission behavior that could lead to the formation of offspring droplets.[25,34] The achieved morphologies and their formation dynamics are consistent with the findings in the literature.[25,57,58]

2.3. PUF Performance. To probe the performance of the fabricated features as a PUF, we calculated the uniformity, uniqueness, reliability, and randomness, which are commonly

https://doi.org/10.1021/acsapm.2c00803
ACS Appl. Polym. Mater. 2022, 4, 5952−5964

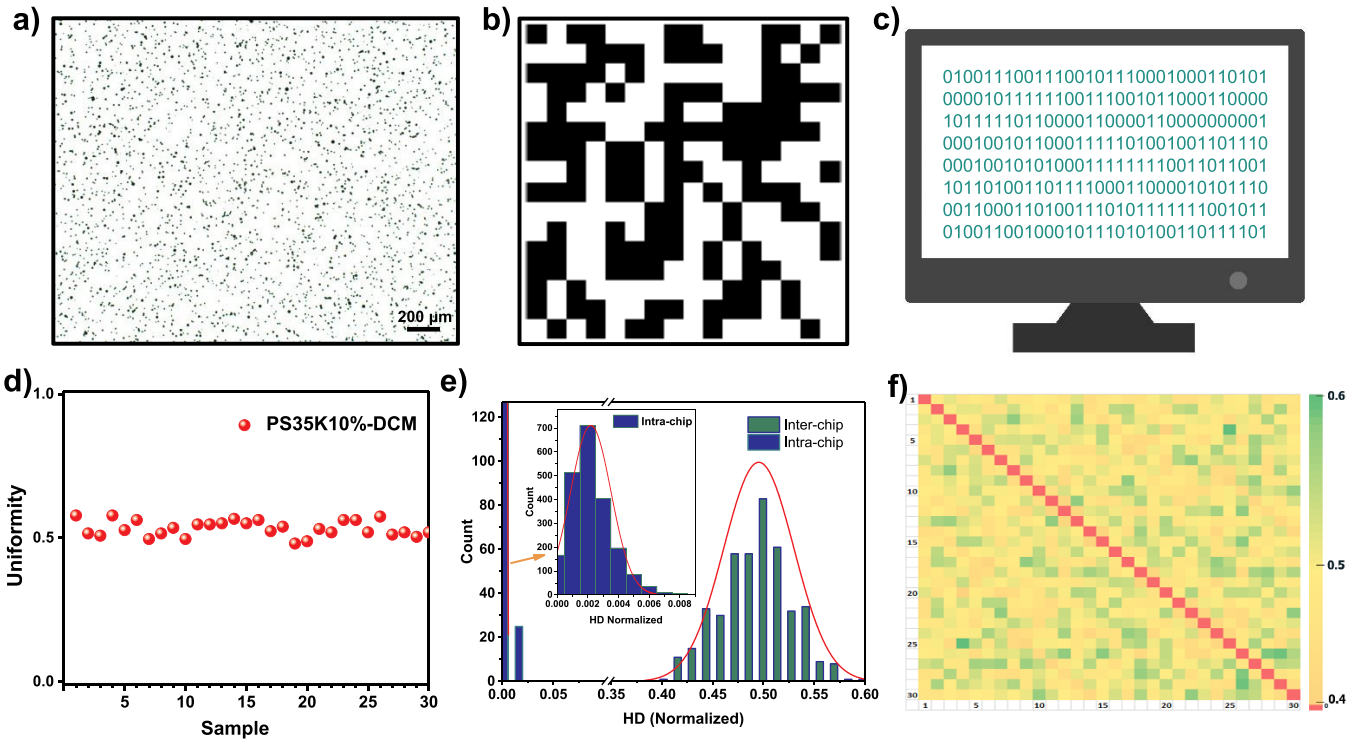

Figure 4. Key generation and extraction of PUF parameters. (a) Representative optical microscopy image of the sample used in the PUF analysis. (b, c) Binarization and size reduction of images for the generation of a security key (0 and 1 bits represent bits of black and white color, respectively). (d) Uniformity of bits obtained from 30 different PUF keys of a PUF chip. (e) HD_{INTRA} and HD_{INTER} distributions. The distributions of HD_{INTRA} and HD_{INTER} are presented on the left and right, respectively. (f) Pairwise comparison map of inter-chip HD values of 30 different PUFs.

accepted as figures of merit. Fine microscopic features obtained by using PS were selected for the PUF performance analysis. This length scale (1−15 μm) is particularly suitable with feature sizes that approach the resolution limit of the portable microscopes, which can even be attached to smartphones. The first step of this analysis is the generation of binary keys from the optical microscopy images (see the Supporting Information for details regarding the extraction of binary keys). A representative optical microscopy image is presented in Figure 4a. The size of this image is reduced to 16 × 16 pixels (Figure 4b). The dark and white pixels in the binarized image correspond to electrosprayed features (0 bits) and the remaining regions (1 bits), respectively. Then, 256 bit long security keys were generated by using these binarized images (Figure 4c). The key generation process was repeated for 30 samples (see the Supporting Information, Figure S5) resulting in 30 different keys. We first calculated the uniformity for each of these keys. The uniformity is a measure of the equal distribution of 1 and 0 bits, with an ideal value of 0.5.[14,59] The uniformity values of our keys ranged between 0.480 and 0.578 with an arithmetic average of 0.533, which was very close to the ideal value (Figure 4d). Another fundamental metric, which has a close relationship with uniformity and also expresses the stochastic distribution of the features, is randomness. We applied the frequency test to all 30 keys for evaluating the randomness.[60] The calculated *p*-value was greater than a value of 0.01 for all samples (Supporting Information, Table S2), implying the stochastic nature of electrosprayed PUFs. Finally, we calculated the uniqueness and reliability. The uniqueness probes the ability to distinguish a PUF from others, and it is calculated based on the Hamming distance.[7,14,60] Ideally, keys generated from any two selected PUFs should not be correlated with each other. On the other hand, reliability is a measure of the repeatability of the responses obtained from a PUF key challenged under different conditions. In Figure 4e, we calculated intra-chip (HD_{INTRA}) and inter-chip Hamming (HD_{INTER}) distance values. The HD_{INTRA} was calculated from images obtained from 30 different PUFs under six different illumination conditions (*i.e.*, contrast and exposure time) for each PUF (see Figure S6 for exemplary images, extracted keys, and illumination conditions). The HD_{INTRA} exhibits a Gaussian distribution with a mean value of 0.0022, which is very close to the ideal value of 0. Meanwhile, the HD_{INTER} calculated from 30 different PUF keys shows a distribution centered at 0.495 with a standard deviation of 0.034, which is close to an ideal value of 0.5, implying the excellent uniqueness for all samples of the PUFs. The intra- and inter-device distributions given in Figure 4e do not overlap, indicating extremely low false positive and negative rates. The false positive and false negative rates obtained with a cutoff threshold of 0.1965 were calculated to be 5.5614×10^{-11} and 2.4749×10^{-12}, respectively. Also, in Figure 4f, a pairwise comparison map of inter-chip HD values was given. The red data on the diagonal show the HD_{INTRA} of identical PUFs, while the other values close to 0.5 correspond to highly uncorrelated HD_{INTER} values. Apart from the representative sample of PS35K-DCM, we also applied the same tests to many other systems to prove that the desired key properties of PUFs can be achieved in different electrosprayed polymer systems. As summarized in Table S3 (Supporting Information), PUF keys generated from other polymers exhibit decent uniformity, uniqueness, and randomness values. All the above findings demonstrate that the electrosprayed PUFs can be employed as a robust security primitive for authentication and anti-counterfeiting.

https://doi.org/10.1021/acsapm.2c00803
ACS Appl. Polym. Mater. 2022, 4, 5952−5964

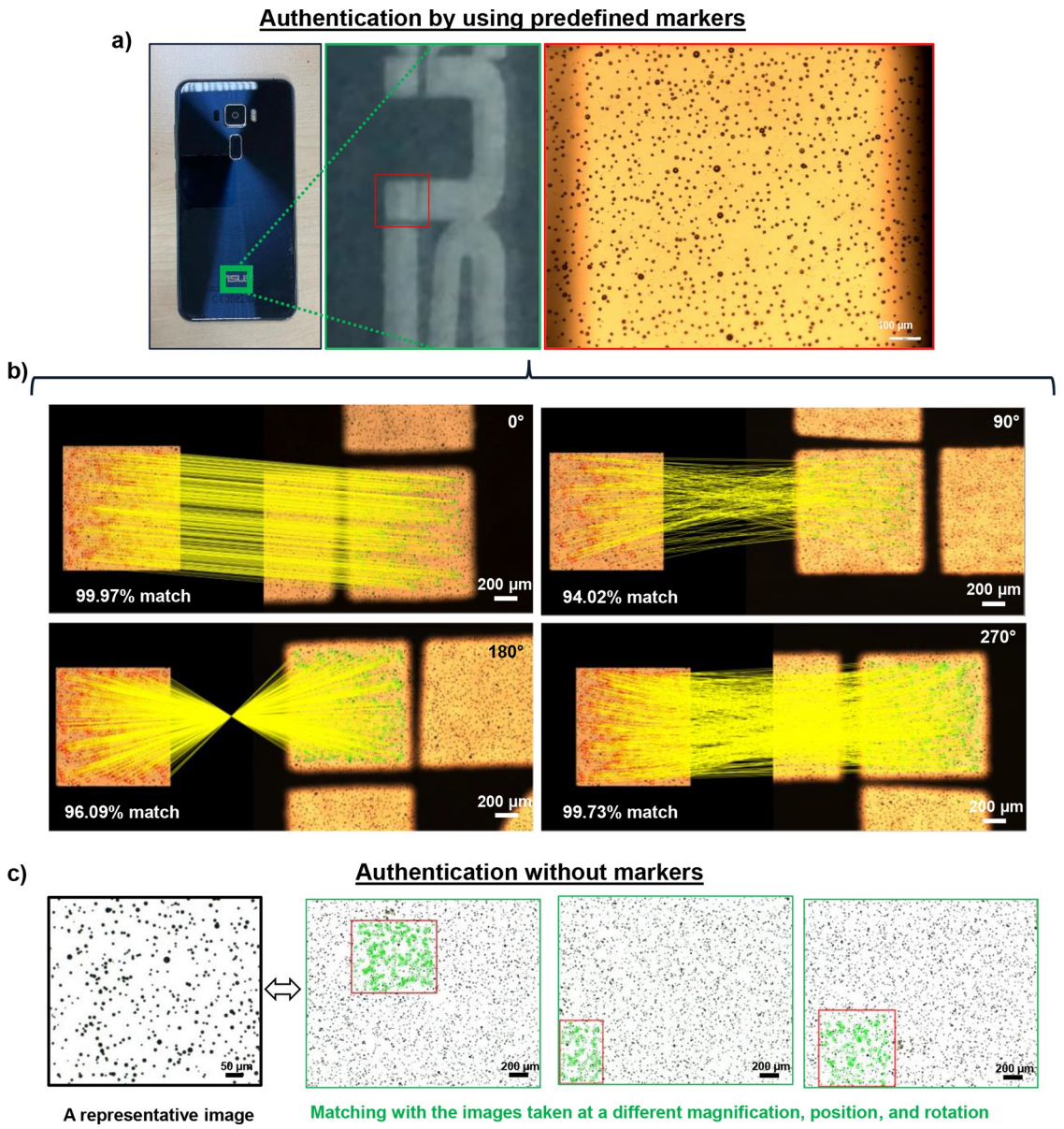

Figure 5. Authentication of electrosprayed PUFs generated from PS35K10%-DCM by using image feature detection algorithms. (a) Photograph of the smartphone on unclonable features is directly formed by electrospraying. The rectangular areas highlighted in green and red show the regions of markers, where the feature matching algorithms were performed. (b) Image authentication, generated from PS35K10%-DCM, using the ORB algorithm and matching scores depending on the rotation angle. The red and green dots on the database and the genuine image are strong feature points that match in both images, and the yellow lines show the positions of these matches. (c) Direct authentication of PUFs without a marker.

2.4. Authentication Using Image Feature Detection Algorithms. The unclonable features fabricated by electrospraying can be directly authenticated using image feature detection algorithms without the need for generating binary keys. In addition to rapid processing, such an approach enables authentication without markers and allows authentication of complex features. Figure 5 presents two different authentication strategies. In the first one, electrosprayed PUFs were directly generated on the label of a real smartphone. This demonstration also shows the practical utilization of the presented approach. The label of the smartphone defined the location of unclonable features. Electrospraying of PS35K10%-DCM solution was then performed directly on the smartphone. The unclonable features on the label were then imaged via an optical microscope and stored in the database. Afterward, the optical microscopy images of the label were taken by rotating the smartphone at angles of 0, 90, 180, and 270°. A feature detection algorithm was then used to match the rotated images with the original image. For this purpose, we used the ORB algorithm implemented in MATLAB. ORB refers to oriented FAST and Rotated BRIEF.[61,62] Here, FAST is a previously reported detection method called as features from accelerated segment test. BRIEF is a feature point descriptor and acronym for binary robust independent elementary features. ORB uses these detector and descriptor algorithms for efficient feature matching with demonstrated capability in a broad range of different fields including PUFs.[53] ORB was highly successful in matching the features for the rotated samples with excellent recognition scores greater than 94%. Figure 5b shows the matching features together with recognition scores and times. An additional advantage of ORB is the recognition speed and computational cost.[61,63] The recognition was performed in 190 ms.

https://doi.org/10.1021/acsapm.2c00803
ACS Appl. Polym. Mater. 2022, 4, 5952−5964

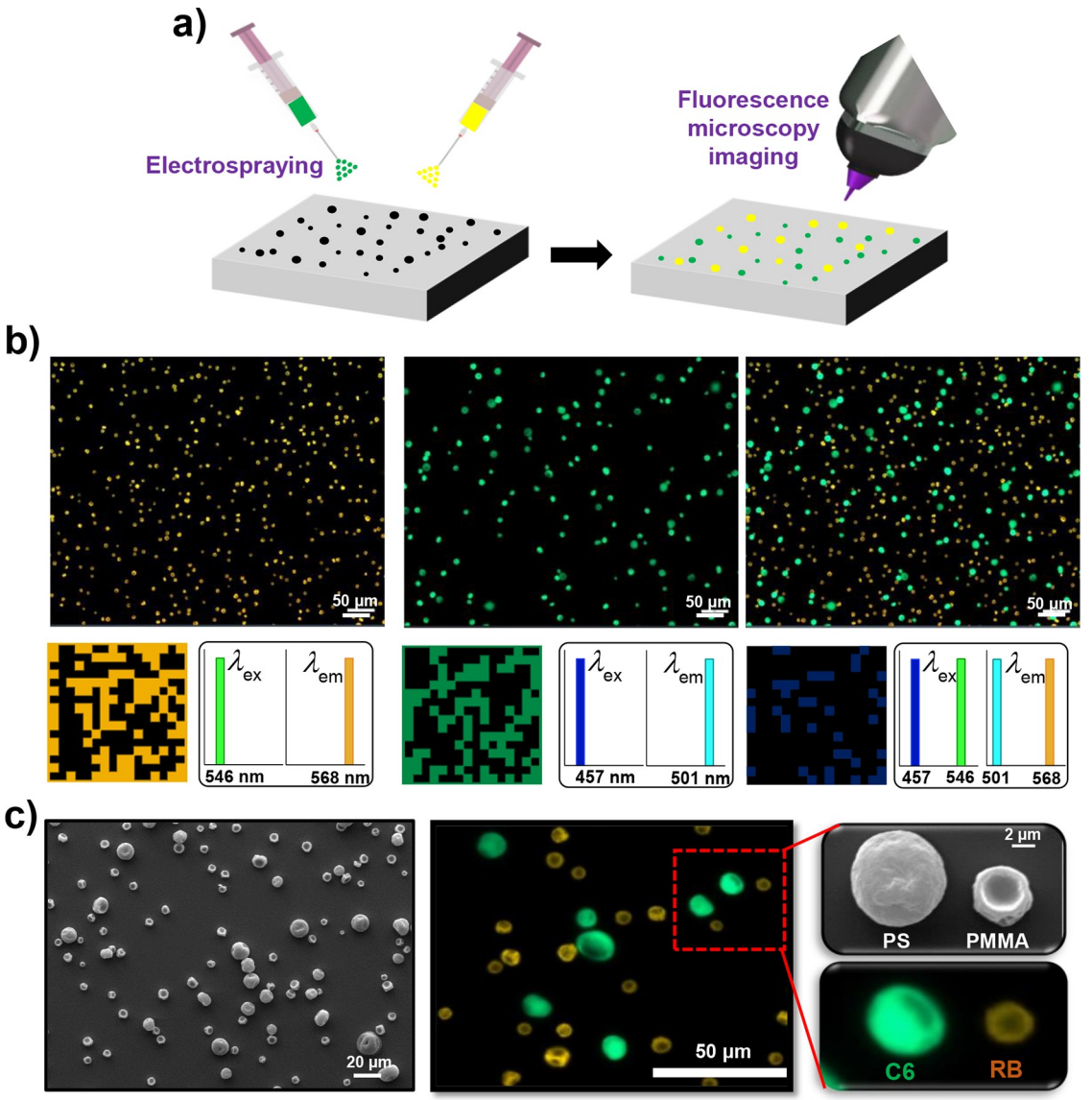

Figure 6. Multiplex deposition of materials. (a) Schematic description and (b) fluorescence microscopy images of the same region obtained with different filters, binary codes extracted from filter-dependent emission color (colored and dark bits refer to 1 and 0 bits, respectively), and representation of specific excitation−emission wavelengths of each fluorescent molecule (for RB and C6). On the right, a merged image, corresponding extracted binary code, and excitation−emission wavelengths are given. (c) SEM and fluorescence microscopy images of the unclonable features with varying characteristics.

A practical concern in the authentication process is constraints that are associated with the imaging conditions, particularly the spatial position of the image. This problem is typically addressed by using physical markers, which could be deposited before or after the PUF fabrication process.[13,50,53,64] Similarly, imaging conditions such as lighting, brightness, contrast, exposure time, and rotation should be well defined for an effective authentication process. Besides the additional fabrication steps, these constraints may result in false negative results for authentic products. To overcome these issues, we used an authentication approach that is independent of the rotation, contrast, scale, and spatial position of the image. We first took optical microscopy images to cover the entire area (10 × 10 mm^2) of the PUF and used these images to form a database. The images were taken at 5× magnification from PUFs fabricated by electrospraying of PS35K-DCM. This process was repeated several times by manually rotating the sample (90, 180, and 270°), and as a result, a total of 134 images were obtained and registered in the database. Test images of unknown authenticity can now be taken at different positions, magnifications, and contrast. By implementing the ORB algorithm, features were determined and compared with those in the database. Figure 5c presents some examples to such an image matching process. The ORB algorithm can effectively match the images, which were taken at different magnifications, rotations, and spatial positions. Even a partial region of the image can be matched in this authentication scheme. The scale, magnification, contrast, and position invariant matching of features are shown in the animation presented in the Video S1. For a fake image that is not registered in the database, there was no matching of features (Figure S7). This authentication has several advantages: (i) There is no need for a physical marker. (ii) The authentication can be performed rapidly by simply taking an image from any position, without restrictions on the

https://doi.org/10.1021/acsapm.2c00803
ACS Appl. Polym. Mater. 2022, 4, 5952−5964

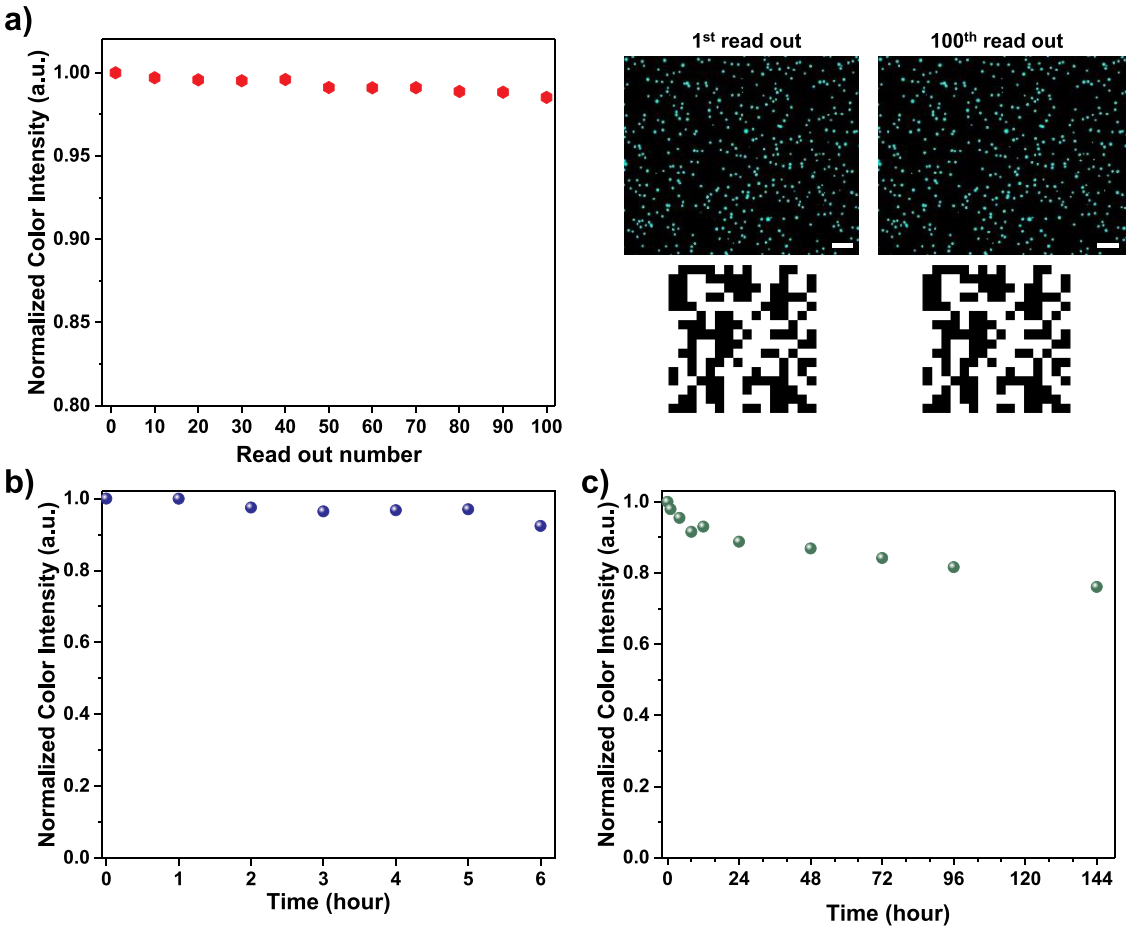

Figure 7. Stability of PUFs. (a) Photostability and read-out stability. The fluorescence intensity as a function of the number of read-out (left) and comparison of fluorescence microscopy images and extracted keys of the 1st and 100th read-out. (Scale bars are 50 μm, and exposure time is 120 ms). (b) Photostability of PUFs under exposure to UV light. The fluorescence intensity as a function of duration of UV light exposure using a source with a power of 3 W at a wavelength of 365 nm. (c) Thermal stability of PUFs. The fluorescence intensity as a function of duration of heating at 50 °C.

magnification, rotation, and imaging conditions. An additional capability is the use of compact and portable microscopy systems for authentication. To demonstrate this capability, we took an image of the fabricated PUF with a handheld optical microscope. This image was successfully matched with the database via the feature matching algorithm (Figure S8). This capability opens up the possibility to incorporate the fabricated PUFs on goods and direct authentication by the end-users without the need for sophisticated tools.

2.5. Multicolor PUFs. An enabling characteristic of electrospraying is the additive deposition of multiple materials on the same substrate. This characteristic is particularly important for establishing additional security layers and increasing the encoding capacity. In addition to augmentation of the complexity, this capability offers multiple authentication pathways. To demonstrate and visualize this capability, we added two different fluorescent organic dyes with distinct photophysical properties to the polymer solutions. Figure 6 presents a summary of the schematics and key results. These polymer solutions doped with fluorescent molecules were then sequentially electrosprayed on the surface (Figure 6a). Advanced electrospraying systems can also achieve simultaneous deposition of multiple materials. Figure 6b shows fluorescence microscopy images of the features fabricated by using PMMA120K-CHF and PS35K-DCM solutions doped with dyes of Rhodamine B (RB) and Coumarin 6 (C6), respectively. The fluorescent molecules have clearly distinct excitation (546 and 457 nm for RB and C6, respectively) and emission wavelengths (568 and 501 nm for RB and C6, respectively), which allow the authentication of features without cross-talk using different filter sets in fluorescence microscopy. Here, both the individual fluorescence images obtained with a particular filter set and merged images can be used to generate keys for authentication. The resulting PUFs can be authenticated at different levels, which can be performed independently. The random distribution of features forms the first level of security, which can be verified by conventional optical microscopy imaging (Figure S9a). The unique morphology of features forms the second security layer, which can be authenticated by using SEM (Figure S9b). For example, PS/C6 (PS with Coumarin 6) leads to plain spherical features, whereas PMMA/RB (PMMA with Rhodamine B) results in cup-like morphology (Figure 6c and Figure S9b). The contrast in the morphology is even discernible in fluorescence microscopy images (Figure 6c). The size of features is also significantly different: 10.9 ± 3.61 μm for PS/C6 and 6.84 ± 1.86 μm for PMMA/RB (Figure S9b).

Finally, we demonstrate the ability to fabricate fluorescent PUFs on different substrates for practical applications. Electrospraying is highly versatile, and any type of material can be used as a substrate. PUFs can be generated even on nonconductive materials, by simply placing the material in front of a conductive

https://doi.org/10.1021/acsapm.2c00803
ACS Appl. Polym. Mater. 2022, 4, 5952−5964

collector and increasing the electrospraying time. Figure S10 presents various demonstrations on flexible substrates and different objects.

2.6. Stability of PUFs. To probe the photostability of fluorescent PUFs fabricated via electrospraying, we performed several different tests. The fluorescent PUFs have remarkable ambient stability as evidenced by fluorescence microscopy images (Figure S11) taken from a sample (PS/C6) stored under atmospheric conditions for more than 7 months. In another experiment, 100 fluorescence microscopy images were captured from the identical location of a sample (Figure 7a and Figure S12). The fluorescence intensity after 100 consecutive imaging was about 98% of the initial intensity, and the keys extracted after the 1st and 100th read-out are almost identical to each other, indicating high levels of read-out stability. To probe the UV light stability, the fabricated PUF was exposed to a light source for several hours (for comparison of fluorescence images, see Figure S13). As given in Figure 7b, the fluorescence intensity measured from the sample after 6 h of UV exposure was more than 90% of the initial value. Figure 7c presents the thermal stability of samples, which were heated to 50 °C up to 6 days. PUFs can completely preserve their morphology without any distortion and exhibit low fluorescence degradation (see Figure S13 for bright field and fluorescence images). The sample retained about ∼87 and ∼76% of its initial fluorescence intensity after 2 and 6 days, respectively.

2.7. Encoding Capacity. The encoding capacity is particularly important to generate keys for large numbers of objects and minimize the trial and error-based replication of the keys. The encoding capacity is defined as k^l, where k is the number of responses ($k = 2$ for binary bits of 0 and 1) and l is the bit size. The proper determination of l is critical for accurate calculation of the encoding capacity. Directly taking the total number of pixels in the image as the value of l can be misleading since each pixel cannot be completely independent from each other. One approach to overcome this issue is the calculation of the degrees of freedom: $l = \mu(1 - \mu)/\sigma^2$, where μ is the mean value and σ is the standard deviation for HD_{INTER}.[14,15,65] For the presented PUF system, the degrees of freedom of the fabricated PUF (given in Figure 4) has a value of ∼216 ($= 0.495 \times (1-0.495)/0.034^2$), which results in an encoding capacity of 2^{216}. The multiplex deposition of features of varying morphology and materials with unique responses offers an unlimited number of options for increasing the encoding capacity. For example, eight different morphologies (Figure 1c) can be doped with two different fluorescent molecules (Figure 6a,b), resulting in 16 different responses and an encoding capacity of 16^l. A key finding here is that such high encoding capacity can be reached by using low-cost bulk materials. Note that the k value can be further increased using additional morphologies, different building blocks such as plasmonic nanoparticles, other types of emitters, and chemicals with unique vibrations.

3. CONCLUSIONS

In summary, these findings establish electrospraying as a viable approach for the effective fabrication of PUFs. The approach is universal and can be readily adapted to a broad range of materials, which is expected to expand the functionality and authentication methods in future studies. The additive operation is key in multiplexing for fabricating encoded surfaces with diverse responses and high encoding capacity. The low-cost, rapid fabrication, and versatility in terms of the substrate are key characteristics of electrospraying for encoding applications. The unique, complex, and 3D morphologies encourage future studies with advanced control over the structure of the features. Various forms of nanomaterials with distinct physical and chemical properties can be incorporated during and post electrospraying. A particularly attractive route is electrospraying of bulk precursors for the in situ synthesis of nanomaterials.

4. EXPERIMENTAL SECTION

4.1. Materials. Silicon wafers (⟨100⟩, N/Phos) were purchased from University Wafer. Poly(ethylene oxide) (PEO) (35 kg/mol), polystyrene (PS) (35 and 280 kg/mol), poly(methyl methacrylate) (PMMA) (120 and 350 kg/mol), and polyvinylpyrrolidone (PVP) (360 and 1300 kg/mol) were purchased from Sigma-Aldrich. Poly(2-vinlypyridine) (P2VP) (40 kg/mol) was purchased from Polysciences Inc. *N*,*N*-Dimethylformamide (DMF), dichloromethane (DCM), chloroform (CHF), and chlorobenzene (CB) were purchased from Sigma-Aldrich. Ethanol was purchased from Merck. Distilled water (DW) was used throughout the experiments. Rhodamine B (RB) and coumarin 6 (C6) were purchased from Sigma-Aldrich.

4.2. Fabrication of Unclonable Features by Electrospraying. To generate random features by electrospraying, solutions were prepared using the polymers listed in Table 1. A range of solvents and their mixtures were used to prepare the solutions. The concentration of the polymer is specified in weight/weight % throughout the manuscript. The solutions were mixed using a magnetic stirrer until the complete dissolution of the polymer. Then, the polymer solutions were electrosprayed onto the surface of the substrates using a commercial electrospinner (Holmarc HO-NFES-040). Unless stated otherwise, the substrate was a silicon wafer. The solutions were placed in a 2.5 mL syringe fitted with a blunt end 18-gauge metallic needle. The syringe was placed in a horizontal configuration against a grounded collector consisting of an aluminum cylinder (75 mm in diameter and 200 mm in length). Silicon substrates were cut into small pieces with a size of 15×15 mm^2 and washed in isopropanol and ethanol followed by UV-ozone treatment. Silicon substrates were taped to the aluminum collector. The tip to the substrate distance was kept constant at 15 cm, and the applied voltage bias was varied between 12 and 15 kV to maintain a single jet. The flow rate was controlled by a syringe pump and varied from 0.5 to 2 mL/h. For the fabrication of fluorescent PUFs, polymer solutions containing 250 μM organic dyes (C6 and RB) were used for electrospraying.

4.3. Characterization. An upright research microscope (ZEISS Axio Imager 2) was used to acquire optical and fluorescence images of the samples. This microscope used a 100 W mercury arc lamb (HBO 100) as the multispectral light source. The fluorescence images of PUFs were acquired by using Filter Set 38 (BP470/40 excitation filter and BP525-550 emission filter) with an FT495 beamsplitter and Filter Set 20 (BP546/12 excitation filter and BP575-640 emission filter) with an FT560 beamsplitter. A portable digital microscope (Dino-Lite Edge, AM7115MZTL) was also used for the practical acquisition of optical bright field images. The morphology of the electrosprayed features was imaged by using scanning electron microscopy (SEM) (Zeiss EVO LS10) operated at 25 kV. The images taken from SEM, optical bright field, and fluorescence microscopy were analyzed by an image analysis program (ImageJ) to determine the statistical distribution of the size of obtained features.

4.4. Image Processing to Extract Binary Keys and Calculation of PUF Parameters. The binary keys and PUF parameters were acquired using MATLAB software. Briefly, original images were binarized. Afterward, 256 (16×16) bit long keys were generated by reducing the size of the original images (for process steps and description, see the Supporting Information and Table S1). The acquired keys were then used to calculate uniformity, uniqueness, randomness, and reliability using the equations given in the Supporting Information.

4.5. Authentication by Feature Detection Algorithms. The ORB (Oriented FAST and Rotated BRIEF) algorithm in MATLAB was used for authentication of PUFs. For the implementation of ORB, the corresponding function of detectORBFeatures was used. The matching

https://doi.org/10.1021/acsapm.2c00803
ACS Appl. Polym. Mater. 2022, 4, 5952−5964

between the captured image and the images in the database was determined by pairwise comparison of the strongest similar points and features identified by the algorithms in both images. The threshold value for the strongest similar points and features was set at 1000. In the first step, the features of the images were extracted with ORB. In the second step, the features obtained from the images were matched with the nearest neighbor-based method. In the third step, mismatches during the matching of key points were cleaned with the RANSAC (random sample consensus) algorithm to determine percentile and mean similarity. In the fourth step, the location information of the remaining features was determined and the features in the images were determined and authenticated. The recognition scores were calculated by the percentile ratio of the number of feature points that were successfully matched to the total number of feature points.

4.6. Stability Tests. To determine the fluorescence stability, 100 fluorescence images were taken from the same position of the sample at 2 min intervals. To probe the UV stability, fluorescence images from the same position of a PUF sample exposed to constant light flux with a peak wavelength of 365 nm and power of 3 W for different durations up to 6 days were collected. Similarly, the emission stability against heat was determined by fluorescence images taken from the same region at certain time intervals from the PUF sample exposed to heat for up to 6 days on a hot plate set at a constant temperature of 50 °C. The reduction in the color intensity in the acquired fluorescence microscopy images was analyzed using the ZEN Blue Lite software of the ZEISS Axio Imager 2 microscope, revealing time-dependent fluorescence stability against light and heat stimuli.

■ ASSOCIATED CONTENT

Supporting Information

The Supporting Information is available free of charge at https://pubs.acs.org/doi/10.1021/acsapm.2c00803.

Animated presentation of the work's scale, magnification, contrast, and position invariant matching (MP4)

Details regarding the process of key extraction, calculation of uniformity, uniqueness, reliability, effects of various parameters on the dimension and morphology of PUFs, additional optical microscopy and SEM images, size distribution histograms, effects of the flow rate, solvent, and composition, PUF performance analysis for different polymer-solvent systems, stability tests, and demonstrations on different goods (PDF)

■ AUTHOR INFORMATION

Corresponding Author

M. Serdar Onses − *ERNAM - Nanotechnology Research and Application Center and Department of Materials Science and Engineering, Erciyes University, Kayseri 38039, Turkey;* orcid.org/0000-0001-6898-7700; Email: onses@erciyes.edu.tr

Authors

Abidin Esidir − *ERNAM - Nanotechnology Research and Application Center and Department of Materials Science and Engineering, Erciyes University, Kayseri 38039, Turkey*

N. Burak Kiremitler − *ERNAM - Nanotechnology Research and Application Center and Department of Materials Science and Engineering, Erciyes University, Kayseri 38039, Turkey;* orcid.org/0000-0001-6065-4899

Mustafa Kalay − *ERNAM - Nanotechnology Research and Application Center, Erciyes University, Kayseri 38039, Turkey; Department of Electricity and Energy, Kayseri University, Kayseri 38039, Turkey*

Alper Basturk − *Department of Computer Engineering and Artificial Intelligence and Big Data Application Research Center, Erciyes University, Kayseri 38039, Turkey*

Complete contact information is available at: https://pubs.acs.org/10.1021/acsapm.2c00803

Notes

The authors declare no competing financial interest.

■ ACKNOWLEDGMENTS

This work was supported by TUBITAK under grant no. 119F384.

■ REFERENCES

(1) Kayaci, N.; Ozdemir, R.; Kalay, M.; Kiremitler, N. B.; Usta, H.; Onses, M. S. Organic Light-Emitting Physically Unclonable Functions. *Adv. Funct. Mater.* **2021**, 2108675.

(2) Arppe-Tabbara, R.; Tabbara, M.; Sørensen, T. J. Versatile and Validated Optical Authentication System Based on Physical Unclonable Functions. *ACS Appl. Mater. Interfaces* **2019**, *11*, 6475−6482.

(3) Davies, J.; Wang, Y. Physically Unclonable Functions (PUFs): A New Frontier in Supply Chain Product and Asset Tracking. *IEEE Eng. Manag. Rev.* **2021**, *49*, 116−125.

(4) Halak, B.; Zwolinski, M.; Mispan, M. S. Overview of PUF-Based Hardware Security Solutions for the Internet of Things. *Midwest Symp. Circuits Syst.* **2016**, *0*, 1−4.

(5) McGrath, T.; Bagci, I. E.; Wang, Z. M.; Roedig, U.; Young, R. J. A PUF Taxonomy. *Appl. Phys. Rev.* **2019**, *6*, No. 011303.

(6) Arppe, R.; Sørensen, T. J. Physical Unclonable Functions Generated through Chemical Methods for Anti-Counterfeiting. *Nat. Rev. Chem.* **2017**, *1*, No. 0031.

(7) Hu, Z.; Comeras, J. M. M. L.; Park, H.; Tang, J.; Afzali, A.; Tulevski, G. S.; Hannon, J. B.; Liehr, M.; Han, S.-J. Physically Unclonable Cryptographic Primitives Using Self-Assembled Carbon Nanotubes. *Nat. Nanotechnol.* **2016**, *11*, 559−565.

(8) Kumar, V.; Dottermusch, S.; Chauhan, A.; Richards, B. S.; Howard, I. A. Expanding the Angle of Incidence Tolerance of Unclonable Anticounterfeiting Labels Based on Microlens Arrays and Luminescent Microparticles. *Adv. Photonics Res.* **2022**, *3*, 2100202.

(9) Tian, L.; Liu, K. K.; Fei, M.; Tadepalli, S.; Cao, S.; Geldmeier, J. A.; Tsukruk, V. V.; Singamaneni, S. Plasmonic Nanogels for Unclonable Optical Tagging. *ACS Appl. Mater. Interfaces* **2016**, *8*, 4031−4041.

(10) Wu, J.; Li, J.; Liu, X.; Gong, L.; Chen, J.; Tang, Z.; Lin, W.; Mu, Y.; Lin, X.; Hong, W.; Yi, G.; Chen, X. Unclonable Photonic Crystal Hydrogels with Controllable Encoding Capacity for Anticounterfeiting. *ACS Appl. Mater. Interfaces* **2022**, *14*, 2369−2380.

(11) Park, J.; Leem, J. W.; Ku, Z.; Kim, J. O.; Chegal, W. C.; Kang, S. W.; Kim, Y. L. Disordered Heteronanostructures of MoS2and TiO2for Unclonable Cryptographic primitives. *ACS Appl. Nano Mater.* **2021**, *4*, 2076−2085.

(12) Caligiuri, V.; Patra, A.; De Santo, M. P.; Forestiero, A.; Papuzzo, G.; Aceti, D. M.; Lio, G. E.; Barberi, R.; De Luca, A. Hybrid Plasmonic/Photonic Nanoscale Strategy for Multilevel Anticounterfeit Labels. *ACS Appl. Mater. Interfaces* **2021**, *13*, 49172−49183.

(13) Kim, J.; Yun, J. M.; Jung, J.; Song, H.; Kim, J. B.; Ihee, H. Anti-Counterfeit Nanoscale Fingerprints Based on Randomly Distributed Nanowires. *Nanotechnology* **2014**, *25*, No. 155303.

(14) Leem, J. W.; Kim, M. S.; Choi, S. H.; Kim, S. R.; Kim, S. W.; Song, Y. M.; Young, R. J.; Kim, Y. L. Edible Unclonable Functions. *Nat. Commun.* **2020**, *11*, 1−11.

(15) Kim, M. S.; Lee, G. J.; Leem, J. W.; Choi, S.; Kim, Y. L.; Song, Y. M. Revisiting Silk: A Lens-Free Optical Physical Unclonable Function. *Nat. Commun.* **2022**, *13*, 1−12.

(16) Hu, Y.-W.; Zhang, T.-P.; Wang, C.-F.; Liu, K.-K.; Sun, Y.; Li, L.; Lv, C.-F.; Liang, Y.-C.; Jiao, F.-H.; Zhao, W.-B.; Dong, L.; Shan, C.-X.; Hu, Y.; Liu, K.; Sun, Y.; Li, L.; Lv, C.; Liang, Y.; Jiao, F.; Zhao, W.; Dong, L.; Shan, C.; Zhang, T.; Wang, C. Flexible and Biocompatible

Physical Unclonable Function Anti-Counterfeiting Label. *Adv. Funct. Mater.* **2021**, *31*, 2102108.
(17) Carro-Temboury, M. R.; Arppe, R.; Vosch, T.; Sørensen, T. J. An Optical Authentication System Based on Imaging of Excitation-Selected Lanthanide Luminescence. *Sci. Adv.* **2018**, *4*, No. e1701384.
(18) Liu, Y.; Han, F.; Li, F.; Zhao, Y.; Chen, M.; Xu, Z.; Zheng, X.; Hu, H.; Yao, J.; Guo, T.; Lin, W.; Zheng, Y.; You, B.; Liu, P.; Li, Y.; Qian, L. Inkjet-Printed Unclonable Quantum Dot Fluorescent Anti-Counterfeiting Labels with Artificial Intelligence Authentication. *Nat. Commun.* **2019**, *10*, 1−9.
(19) Zheng, X.; Zhu, Y.; Liu, Y.; Zhou, L.; Xu, Z.; Feng, C.; Zheng, C.; Zheng, Y.; Bai, J.; Yang, K.; Zhu, D.; Yao, J.; Hu, H.; Zheng, Y.; Guo, T.; Li, F. Inkjet-Printed Quantum Dot Fluorescent Security Labels with Triple-Level Optical Encryption. *ACS Appl. Mater. Interfaces* **2021**, *13*, 15701−15708.
(20) Chen, F.; Li, Q.; Li, M.; Huang, F.; Zhang, H.; Kang, J.; Wang, P. Unclonable Fluorescence Behaviors of Perovskite Quantum Dots/Chaotic Metasurfaces Hybrid Nanostructures for Versatile Security Primitive. *Chem. Eng. J.* **2021**, *411*, No. 128350.
(21) Liu, Y.; Zheng, Y.; Zhu, Y.; Ma, F.; Zheng, X.; Yang, K.; Zheng, X.; Xu, Z.; Ju, S.; Zheng, Y.; Guo, T.; Qian, L.; Li, F. Unclonable Perovskite Fluorescent Dots with Fingerprint Pattern for Multilevel Anticounterfeiting. *ACS Appl. Mater. Interfaces* **2020**, *12*, 39649−39656.
(22) Chen, X.; Wang, K.; Shi, B.; Liu, T.; Chen, R.; Zhang, M.; Wen, W.; Xing, G.; Wu, J. All-Inorganic Perovskite Nanorod Arrays with Spatially Randomly Distributed Lasing Modes for All-Photonic Cryptographic Primitives. *ACS Appl. Mater. Interfaces* **2021**, *13*, 30891−30901.
(23) Gan, Z.; Chen, F.; Li, Q.; Li, M.; Zhang, J.; Lu, X.; Tang, L.; Wang, Z.; Shi, Q.; Zhang, W.; Huang, W. Reconfigurable Optical Physical Unclonable Functions Enabled by VO2 Nanocrystal Films. *ACS Appl. Mater. Interfaces* **2022**, 5785.
(24) Fernández-Benito, A.; Hoyos, M.; López-Manchado, M. A.; Sørensen, T. J.A Physical Unclonable Function Based on Recyclable Polymer Nanoparticles to Enable the Circular Economy. *ACS Appl. Nano Mater.* 2022, .
(25) Bodnár, E.; Grifoll, J.; Rosell-Llompart, J. Polymer Solution Electrospraying: A Tool for Engineering Particles and Films with Controlled Morphology. *J. Aerosol Sci.* **2018**, *125*, 93−118.
(26) Xie, J.; Jiang, J.; Davoodi, P.; Srinivasan, M. P.; Wang, C. H. Electrohydrodynamic Atomization: A Two-Decade Effort to Produce and Process Micro-/Nanoparticulate Materials. *Chem. Eng. Sci.* **2015**, *125*, 32−57.
(27) He, T.; Jokerst, J. V. Structured Micro/Nano Materials Synthesized via Electrospray: A Review. *Biomater. Sci.* **2020**, *8*, 5555−5573.
(28) Khalily, M. A.; Yurderi, M.; Haider, A.; Bulut, A.; Patil, B.; Zahmakiran, M.; Uyar, T. Atomic Layer Deposition of Ruthenium Nanoparticles on Electrospun Carbon Nanofibers: A Highly Efficient Nanocatalyst for the Hydrolytic Dehydrogenation of Methylamine Borane. *ACS Appl. Mater. Interfaces* **2018**, *10*, 26162−26169.
(29) Vempati, S.; Ranjith, K. S.; Topuz, F.; Biyikli, N.; Uyar, T. Electrospinning Combined with Atomic Layer Deposition to Generate Applied Nanomaterials: A Review. *ACS Appl. Nano Mater.* **2020**, *3*, 6186−6209.
(30) Huang, C.; Lucas, B.; Vervaet, C.; Braeckmans, K.; Van Calenbergh, S.; Karalic, I.; Vandewoestyne, M.; Deforce, D.; Demeester, J.; De Smedt, S. C. Unbreakable Codes in Electrospun Fibers: Digitally Encoded Polymers to Stop Medicine Counterfeiting. *Adv. Mater.* **2010**, *22*, 2657−2662.
(31) Bai, J.; Tian, Y.; Wang, Y.; Fu, J.; Cheng, Y.; Qiang, S.; Yu, D.; Zhang, W.; Yuan, K.; Chai, X. Exploring Electrospun Nanofibers for Physically Unclonable Functions: A Scalable and Robust Method toward Unique Identifiers. *J. Phys. D: Appl. Phys.* **2022**, *55*, 205106.
(32) Taşcioğlu, D.; Atçi, A.; Ünlütürk, S. S.; Özçelik, S. Physically Unclonable Security Patterns Created by Electrospinning, and Authenticated by Two-Step Validation Method. *Nanotechnology* **2022**, *33*, No. 095302.
(33) Feng, Y.; Gu, Y.; Wang, M.; Xu, X.; Liu, Y.; Li, D.; Feng, Y.; Gu, Y.; Wang, M.; Xu, X.; Li, D.; Liu, Y. Plasmonic Anti-Counterfeiting Labels Based on the Au@SiO2-Embedded Electrospun Fibers. *Adv. Mater. Interfaces* **2021**, *8*, 2002246.
(34) Gañán-Calvo, A. M.; López-Herrera, J. M.; Herrada, M. A.; Ramos, A.; Montanero, J. M. Review on the Physics of Electrospray: From Electrokinetics to the Operating Conditions of Single and Coaxial Taylor Cone-Jets, and AC Electrospray. *J. Aerosol Sci.* **2018**, *125*, 32−56.
(35) Jaworek, A. Electrohydrodynamic Microencapsulation Technology. *Encapsulations* **2016**, 1−45.
(36) Abdelazim, N. M.; Fong, M. J.; McGrath, T.; Woodhead, C. S.; Al-Saymari, F.; Bagci, I. E.; Jones, A. T.; Wang, X.; Young, R. J. Hotspot Generation for Unique Identification with Nanomaterials. *Sci. Rep.* **2021**, *11*, 1−7.
(37) Taylor, G. Electrically Driven Jets. *Proc. R. Soc. A Math. Phys. Eng. Sci.* **1969**, *313*, 453−475.
(38) Frs, L. On the Equilibrium of Liquid Conducting Masses Charged with Electricity. 2009, *14* (87), 184−186, .
(39) Brandenberger, H.; Nüssli, D.; Piēch, V.; Widmer, F. Monodisperse Particle Production: A Method to Prevent Drop Coalescence Using Electrostatic Forces. *J. Electrostat.* **1999**, *45*, 227−238.
(40) Jaworek, A.; Sobczyk, A. T. Electrospraying Route to Nanotechnology: An Overview. *J. Electrostat.* **2008**, *66*, 197−219.
(41) Ozcan, A. Mobile Phones Democratize and Cultivate Next-Generation Imaging. Diagnostics and Measurement Tools. *Lab Chip* **2014**, *14*, 3187−3194.
(42) Contreras-Naranjo, J. C.; Wei, Q.; Ozcan, A. Mobile Phone-Based Microscopy, Sensing, and Diagnostics. *IEEE J. Sel. Top. Quantum Electron* **2016**, *22*, 1−14.
(43) Jing, L.; Xie, Q.; Li, H.; Li, K.; Yang, H.; Ng, P. L. P.; Li, S.; Li, Y.; Teo, E. H. T.; Wang, X.; Chen, P. Y. Multigenerational Crumpling of 2D Materials for Anticounterfeiting Patterns with Deep Learning Authentication. *Matter* **2020**, *3*, 2160−2180.
(44) Jouyban, A.; Soltanpour, S.; Chan, H. K. A Simple Relationship between Dielectric Constant of Mixed Solvents with Solvent Composition and Temperature. *Int. J. Pharm.* **2004**, *269*, 353−360.
(45) Park, C. H.; Lee, J. Electrosprayed Polymer Particles: Effect of the Solvent Properties. *J. Appl. Polym. Sci.* **2009**, *114*, 430−437.
(46) Onses, M. S.; Sutanto, E.; Ferreira, P. M.; Alleyne, A. G.; Rogers, J. A. Mechanisms, Capabilities, and Applications of High-Resolution Electrohydrodynamic Jet Printing. *Small* **2015**, *11*, 4237−4266.
(47) Gañán-Calvo, A. M.; Dávila, J.; Barrero, A. Current and Droplet Size in the Electrospraying of Liquids. Scaling Laws. *J. Aerosol Sci.* **1997**, *28*, 249−275.
(48) Kurakula, M.; Koteswara Rao, G. S. N. Moving Polyvinyl Pyrrolidone Electrospun Nanofibers and Bioprinted Scaffolds toward Multidisciplinary Biomedical Applications. *Eur. Polym. J.* **2020**, *136*, No. 109919.
(49) Knop, K.; Hoogenboom, R.; Fischer, D.; Schubert, U. S. Poly(Ethylene Glycol) in Drug Delivery: Pros and Cons as Well as Potential Alternatives. *Angew. Chem., Int. Ed.* **2010**, *49*, 6288−6308.
(50) Torun, N.; Torun, I.; Sakir, M.; Kalay, M.; Onses, M. S. Physically Unclonable Surfaces via Dewetting of Polymer Thin Films. *ACS Appl. Mater. Interfaces* **2021**, *13*, 11247−11259.
(51) Kiremitler, N. B.; Torun, I.; Altintas, Y.; Patarroyo, J.; Demir, H. V.; Puntes, V. F.; Mutlugun, E.; Onses, M. S. Writing Chemical Patterns Using Electrospun Fibers as Nanoscale Inkpots for Directed Assembly of Colloidal Nanocrystals. *Nanoscale* **2020**, *12*, 895−903.
(52) Malynych, S.; Luzinov, I.; Chumanov, G. Poly(Vinyl Pyridine) as a Universal Surface Modifier for Immobilization of NanoparticlesMalynych, S., Luzinov, I., & Chumanov, G. Poly(Vinyl Pyridine) as a Universal Surface Modifier for Immobilization of Nanoparticles. *J. Phys. Chem. B* **2002**, *106*, 1280−1285.
(53) Chen, G.; Weng, Y.; Wang, W.; Hong, D.; Zhou, L.; Zhou, X.; Wu, C.; Zhang, Y.; Yan, Q.; Yao, J.; Guo, T. Spontaneous Formation of Random Wrinkles by Atomic Layer Infiltration for Anticounterfeiting. *ACS Appl. Mater. Interfaces* **2021**, *13*, 27548−27556.

(54) Ma, T.; Li, T.; Zhou, L.; Ma, X.; Yin, J.; Jiang, X. Dynamic Wrinkling Pattern Exhibiting Tunable Fluorescence for Anticounterfeiting Applications. *Nat. Commun.* **2020**, *11*, 1−8.
(55) Barton, A. F. M. *CRC Handbook of Solubility Parameters and Other Cohesion Parameters*; Second Ed. 2017, 1−739, .
(56) Hansen, C. M. *Hansen Solubility Parameters : A User's Handbook*; Second Edition. 2007, 113−123, .
(57) Liu, J.; Kumar, S. Microscopic Polymer Cups by Electrospinning. *Polymer* **2005**, *46*, 3211−3214.
(58) Eda, G.; Shivkumar, S. Bead Structure Variations during Electrospinning of Polystyrene. *J. Mater. Sci.* **2006**, *41*, 5704−5708.
(59) Maiti, A.; Gunreddy, V.; Schaumont, P. A Systematic Method to Evaluate and Compare the Performance of Physical Unclonable Functions. *Embed. Syst. Des. with FPGAs* **2013**, 245−267.
(60) Rukhin, A.; Soto, J.; Nechvatal, J.; Smid, M.; Barker, E.; Leigh, S.; Levenson, M.; Vangel, M.; Banks, D.; Heckert, A.; Dray, J.; Vo, S. *Special Publication 800−22 Revision 1a A Statistical Test Suite for Random and Pseudorandom Number Generators for Cryptographic Applications*, .
(61) Rublee, E.; Rabaud, V.; Konolige, K.; Bradski, G. ORB: An Efficient Alternative to SIFT or SURF. *Proc. IEEE Int. Conf. Comput. Vis.* **2011**, 2564−2571.
(62) Calonder, M.; Lepetit, V.; Strecha, C.; Fua, P. BRIEF: Binary Robust Independent Elementary Features. *Lect. Notes Comput. Sci.* **2010**, 778−792.
(63) Tareen, S. A. K.; Saleem, Z. A Comparative Analysis of SIFT, SURF, KAZE, AKAZE, ORB, and BRISK. *Int. Conf. Comput. Math. Eng. Technol. Inven. Innov. Integr. Socioecon. Dev. iCoMET 2018 − Proc.* **2018**, 1−10.
(64) Zheng, Y.; Jiang, C.; Ng, S. H.; Lu, Y.; Han, F.; Bach, U.; Gooding, J. J. Unclonable Plasmonic Security Labels Achieved by Shadow-Mask-Lithography-Assisted Self-Assembly. *Adv. Mater.* **2016**, *28*, 2330−2336.
(65) Pappu, R.; Recht, B.; Taylor, J.; Gershenfeld, N. Physical One-Way Functions. *Science* **2002**, *297*, 2026−2030.

https://doi.org/10.1021/acsapm.2c00803
ACS Appl. Polym. Mater. 2022, 4, 5952−5964